Supplementary figures

a

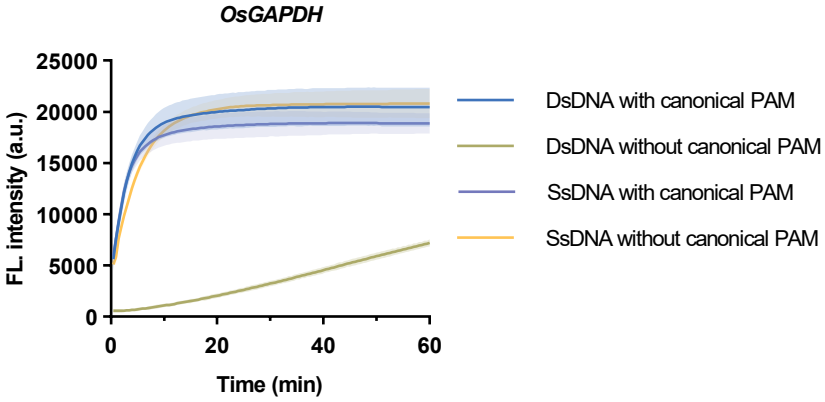

b

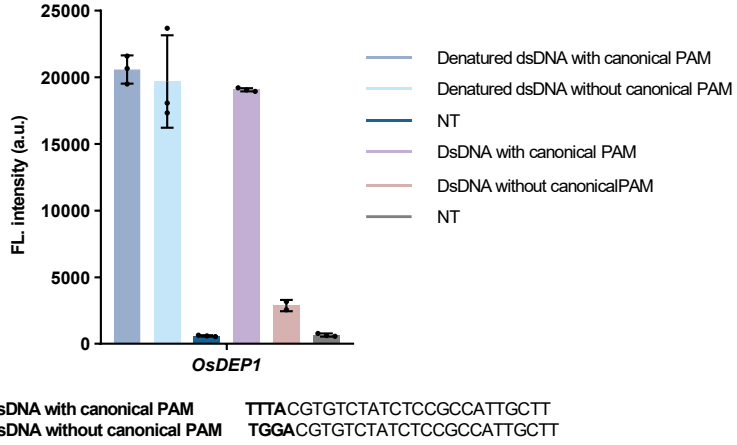

Fig. S1. Fluorescence signals of Cas12a for ssDNA/dsDNA detection both with or without canonical PAM motifs. a, Assessment of LbCas12a trans-cleavage activity using artificially synthesized dsDNA and ssDNA, both substrates with or without canonical PAM motifs at *OsGAPDH* site. b, Fluorescence signals of *OsDEP1* site (corresponding to results in Fig. 1c) following 1-hour incubation in the detection system. NT represents PCR products with non-target DNA. Fluorescence intensities (mean ± *s.d.*) were calculated from three independent experiments (n = 3) and quantified in arbitrary units (a.u.).

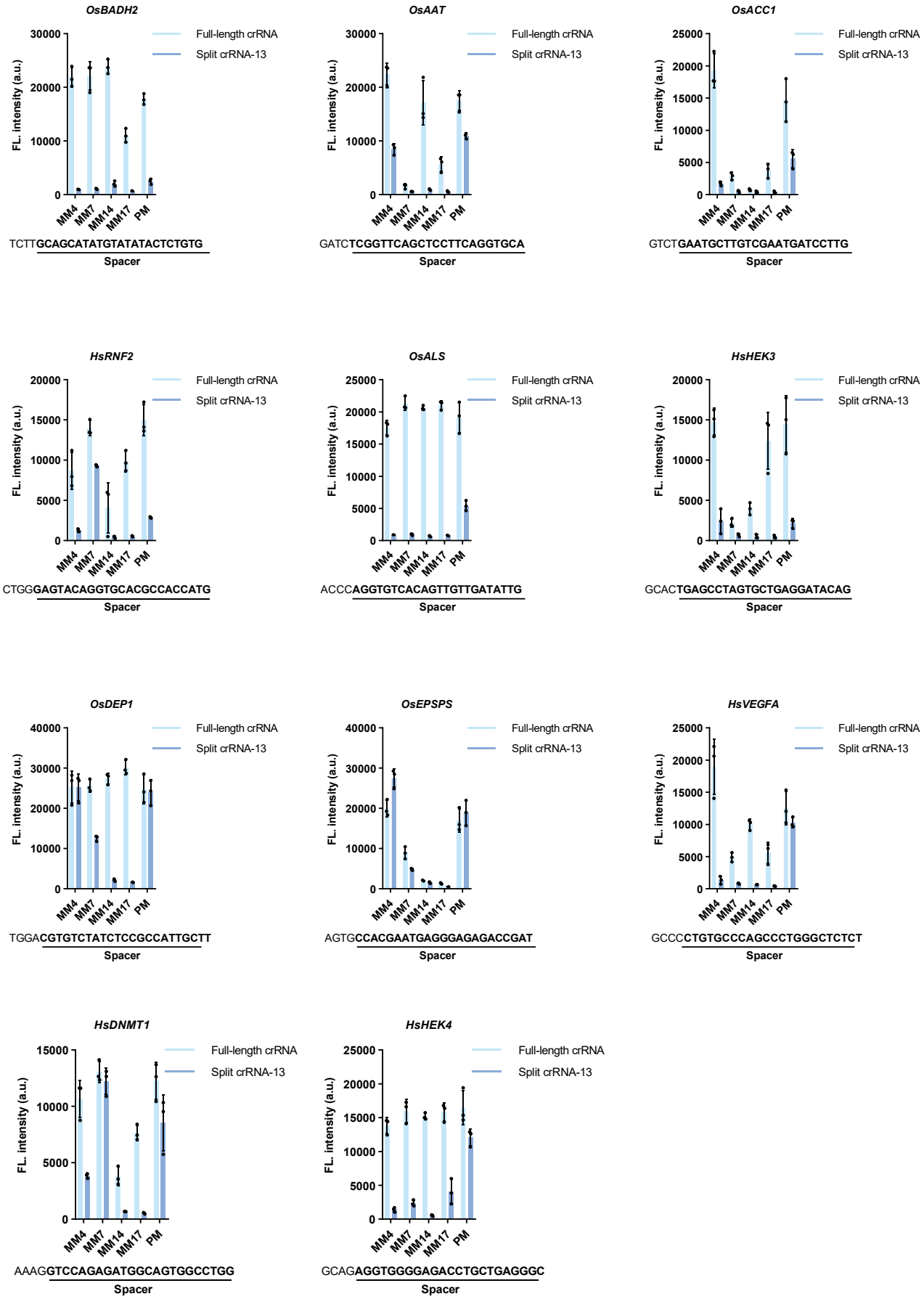

Fig. S2. Fluorescence signals of Cas12a detection for single-nucleotide mismatch targets using full-length crRNA or split crRNA. The effects of mismatch position of split crRNA-13 and full-length crRNA were evaluated. Single-nucleotide mismatches at protospacer location +4 (MM4), +7 (MM7), +14 (MM14), and +17 (MM17) were showed. PM: perfect match targets; MM: mismatch targets. Fluorescence intensities (mean ± *s.d.*) were calculated from three independent experiments (n = 3) and quantified in arbitrary units (a.u.).

a

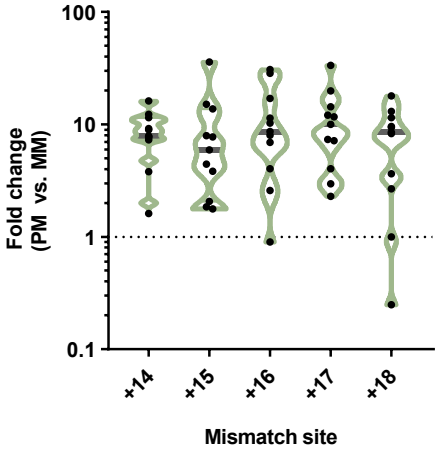

b

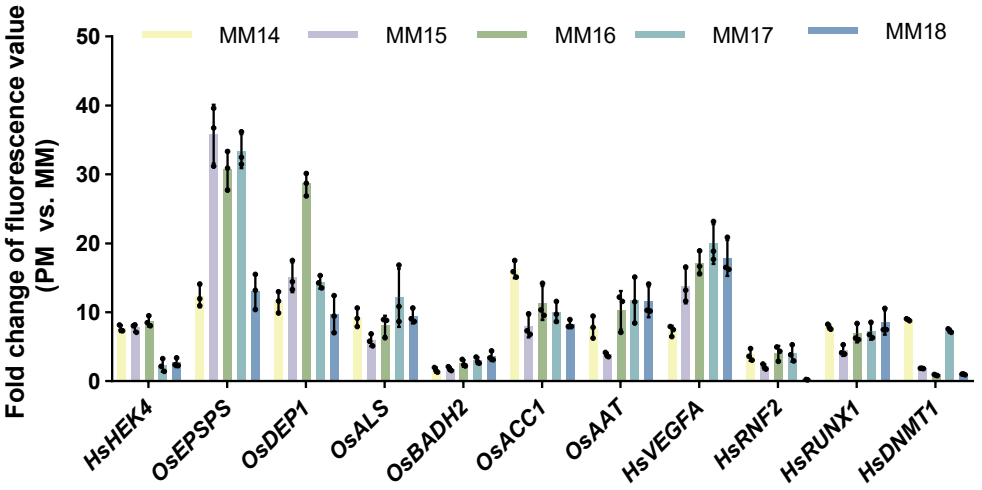

Fig. S3. Ratio of fluorescence signals between perfect-match and mismatch targets measured by the SNIPER assay. a, Ratios are showed for the wild-type spacer sequence relative to spacer sequences containing a single SNP at position +14, +15, +16, +17, or +18. b, The ratios of PM and MM for each corresponding position. PM, perfect match target; MM, mismatch target.

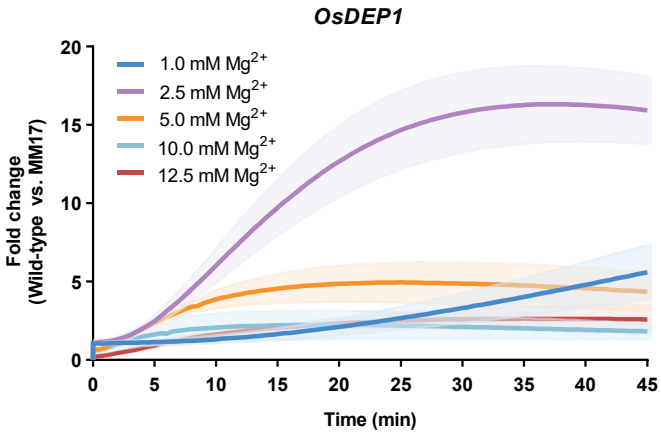

Fig. S4. Effects of Mg^{2+} concentration on SNIPER assay performance. Comparative analysis of detection efficiency at Mg^{2+} concentrations of 1.0 mM, 2.5 mM, 5.0 mM, 10.0 mM and 12.5 mM in the SNIPER system. The X-axis represents incubation time, with fluorescence signal recorded every 30 s. The Y-axis represents the fold change of wild type versus MM17.

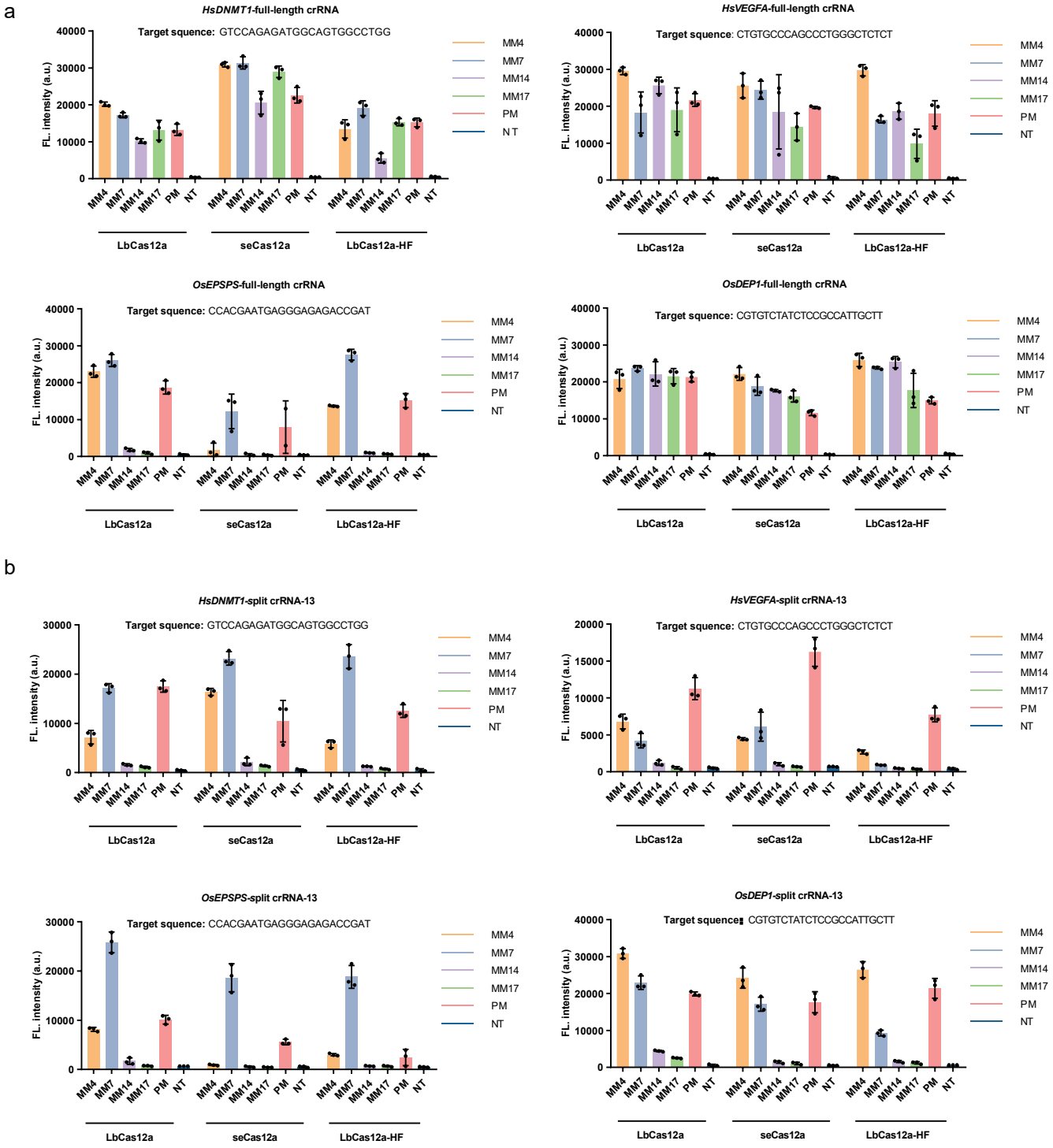

Fig. S5. Performance of full-length crRNA and split crRNA in SNP discrimination across four genomic loci using different Cas12a variants (LbCas12a, seCas12a, LbCas12a-HF). a, Effects of SNPs at positions +4, +7, +14, and +17 within the spacer sequence of full-length crRNA; b, Effect of SNPs at positions +4, +7, +14, and +17 within the spacer sequence of split crRNA. NT represents PCR products with non-target DNA. Fluorescence intensities (mean ± *s.d.*) were calculated from three independent experiments (n = 3) and quantified in arbitrary units (a.u.).

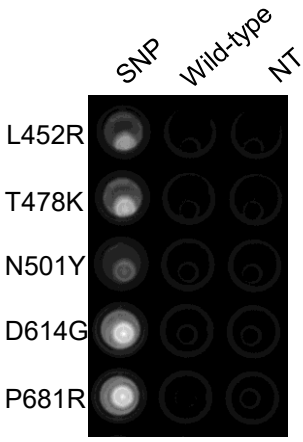

Fig. S6. Visualized analysis under UV illumination of SARS-CoV-2 variant detection using the SNIPER assay. This figure corresponds to the results in Fig. 3b. NT represents PCR products with non-target DNA.

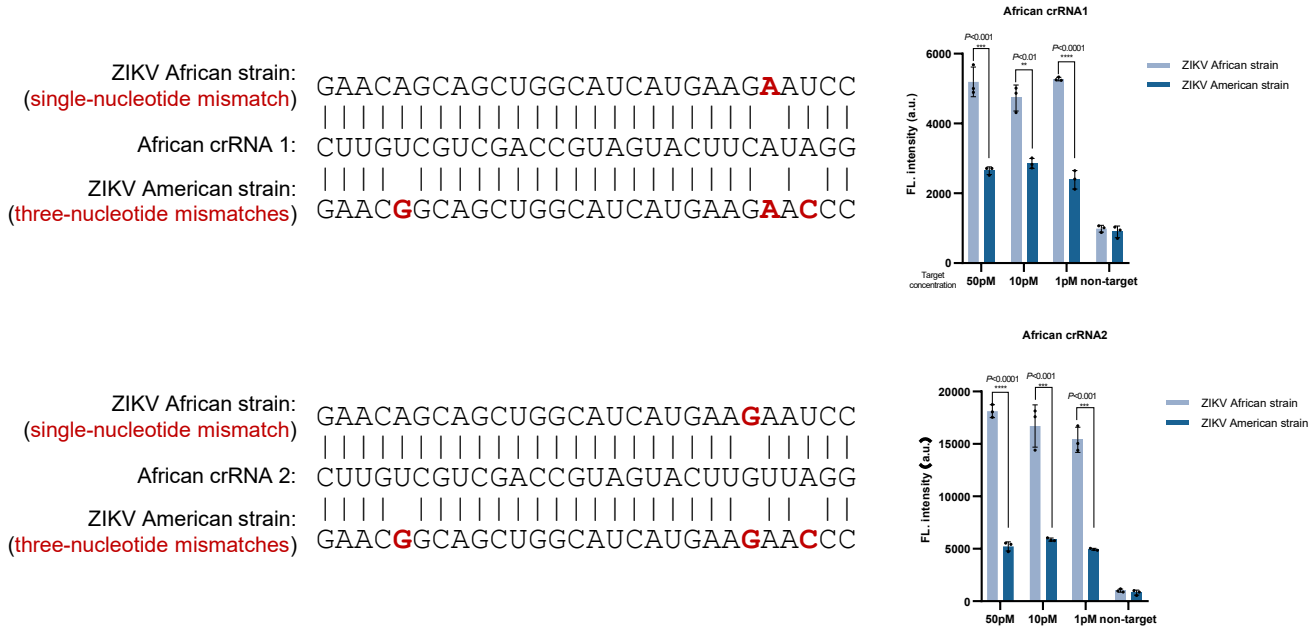

Fig. S7. SHERLOCK for variants detection results of Zika virus (ZIKV) African strain and American strain. The target sequences, crRNA designs and experimental procedure fully follow the procedure described in the original study. Left: The sequences displayed the crRNA spacer sequences and the corresponding DNA target sequences of the two strains. For the African strain, crRNA paired with the target sequences with single-nucleotide mismatches; For the American strain, crRNA paired with the target sequences with three-nucleotide mismatches. Right: The bar graphs show the fluorescence intensities detected by SHERLOCK for African crRNA1 and African crRNA2 when paired with both the African and American strains. Fluorescence intensities (mean ± *s.d.*) were calculated from three independent experiments (n = 3) and quantified in arbitrary units (a.u.). P values were obtained using the two-tailed Student's t-test. *$P < 0.05$, **$P < 0.01$, ***$P < 0.001$, ****$P < 0.0001$, n.s., $P > 0.05$.

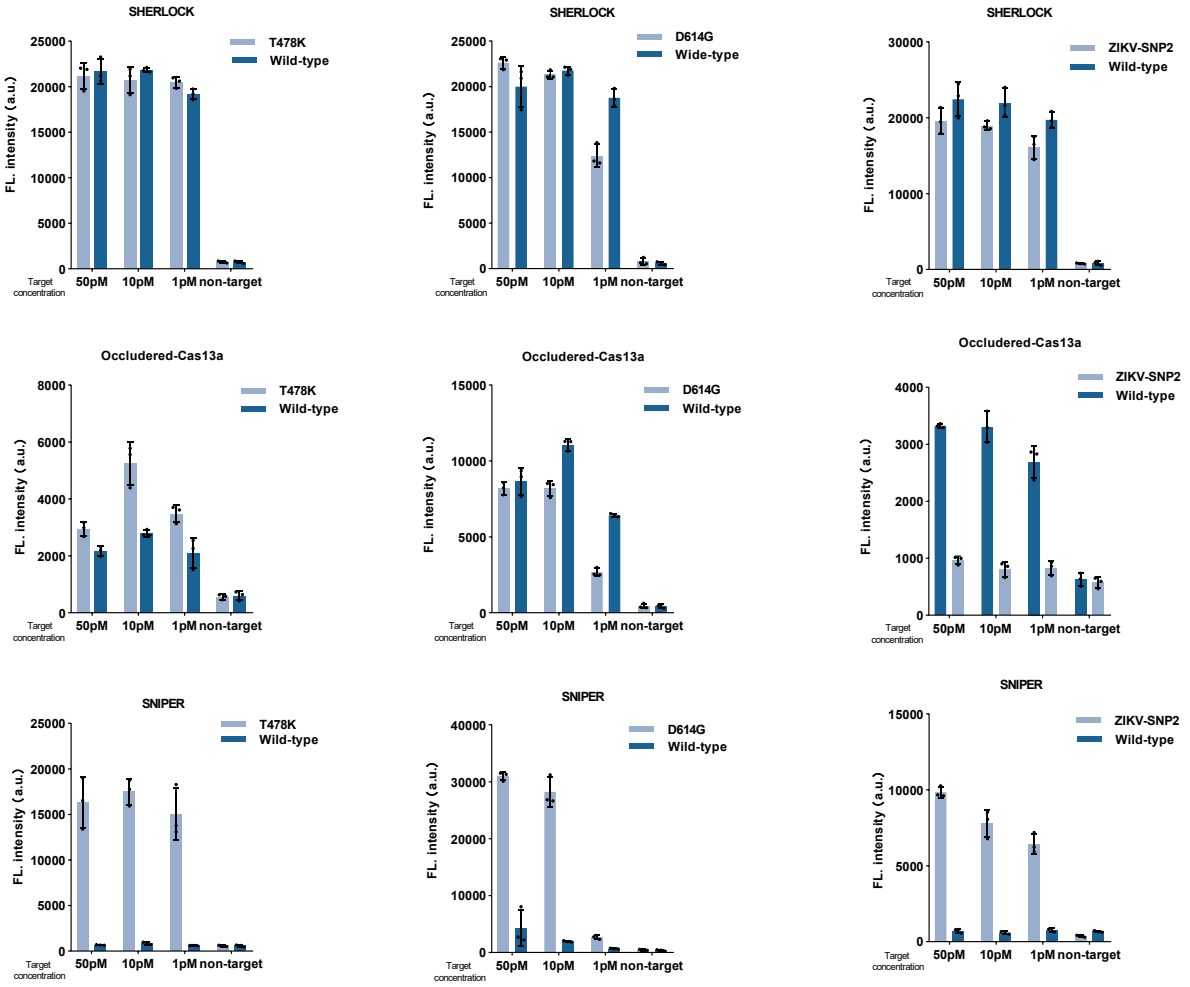

Fig. S8. Comparison of SNP detection results among SNIPER, SHERLOCK and Occludered-Cas13a assays at different target concentrations. Fluorescence intensities (mean ± *s.d.*) were calculated from three independent experiments (*n* = 3) and quantified in arbitrary units (a.u.).

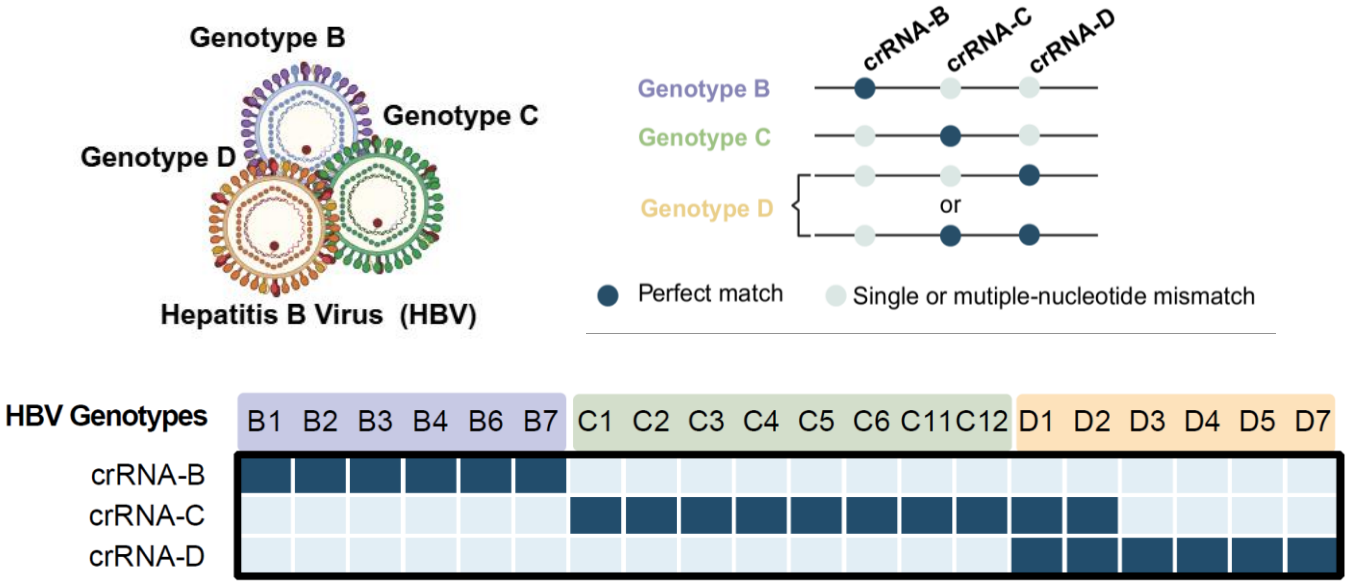

Fig. S9. Schematic diagram of the SNIPER assay for HBV genotyping. Three crRNAs were used to differentiate HBV genotypes B, C, and D via SNIPER assay. Dark blue blocks represent positive fluorescence readouts for HBV subtyping with the corresponding crRNA.

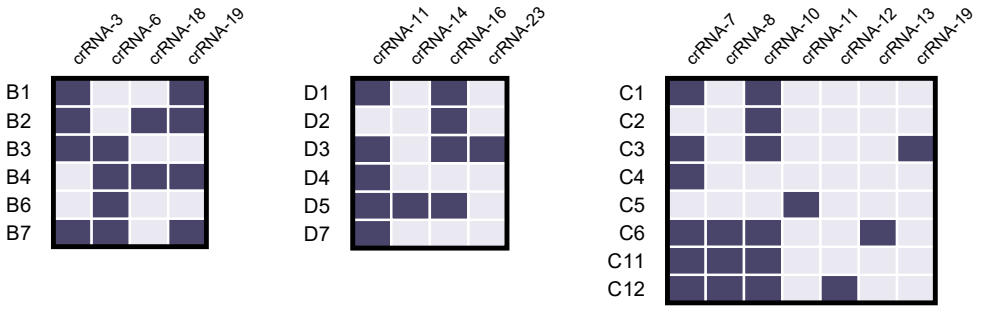

Fig. S10. SNIPER for distinguishing HBV subtypes. Different HBV subtypes are indicated on the left side of the figure. Drak blue blocks represent positive SNIPER signals.

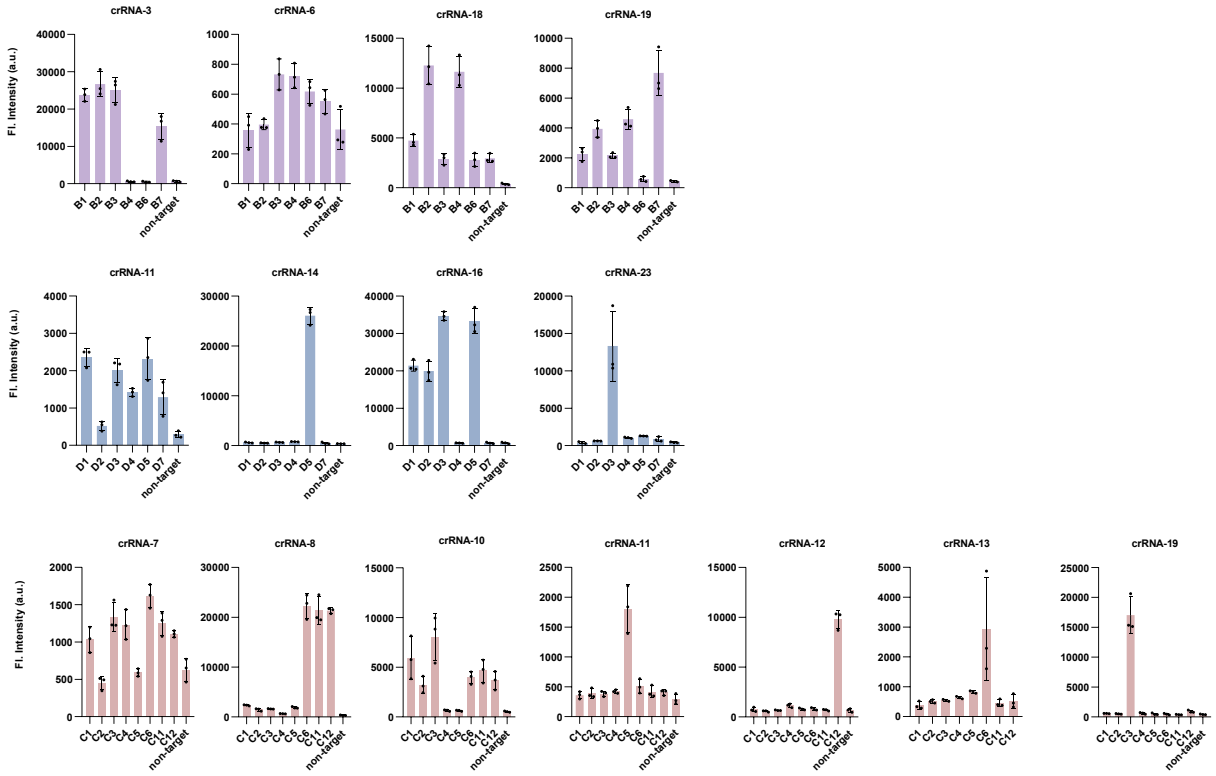

Fig. S11. Fluorescence signal of SNIPER for genotyping of HBV subtypes. The X-axis represents various HBV subgenotypes. Distinct crRNAs were designed to target different SNP loci. These panels correspond to those in Fig. S10. Fluorescence intensities (mean ± *s.d.*) were calculated from three independent experiments (n = 3) and quantified in arbitrary units (a.u.).

a

HsPNPLA3 (c.444C>G & c.447C>T)

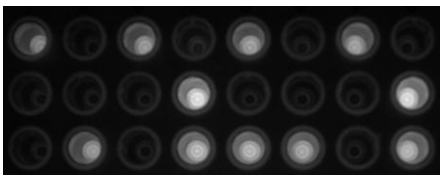

#1-8

#9-16

#17-24

b

*HsALDH2*2* (c.1510G>A)

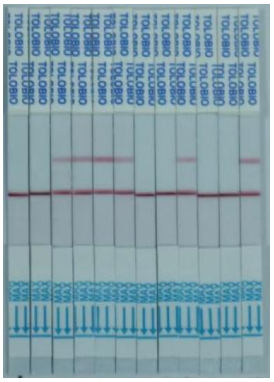

#1-12

Fig. S12. Visualization results of SNP genotyping of *HsPNPLA3* and *HsALDH2*2* in clinical samples. a, Visualization results of partial samples under UV light via SNIPER assay. b, The discrimination results readout using the LFA assay for representative samples. Fluorescence intensities (mean ± *s.d.*) were calculated from three independent experiments (*n* = 3) and quantified in arbitrary units (a.u.).

a

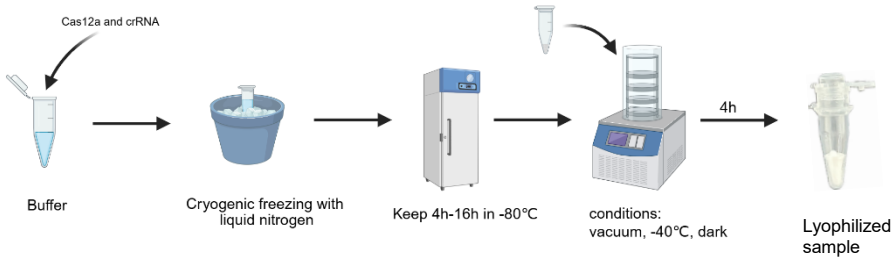

b

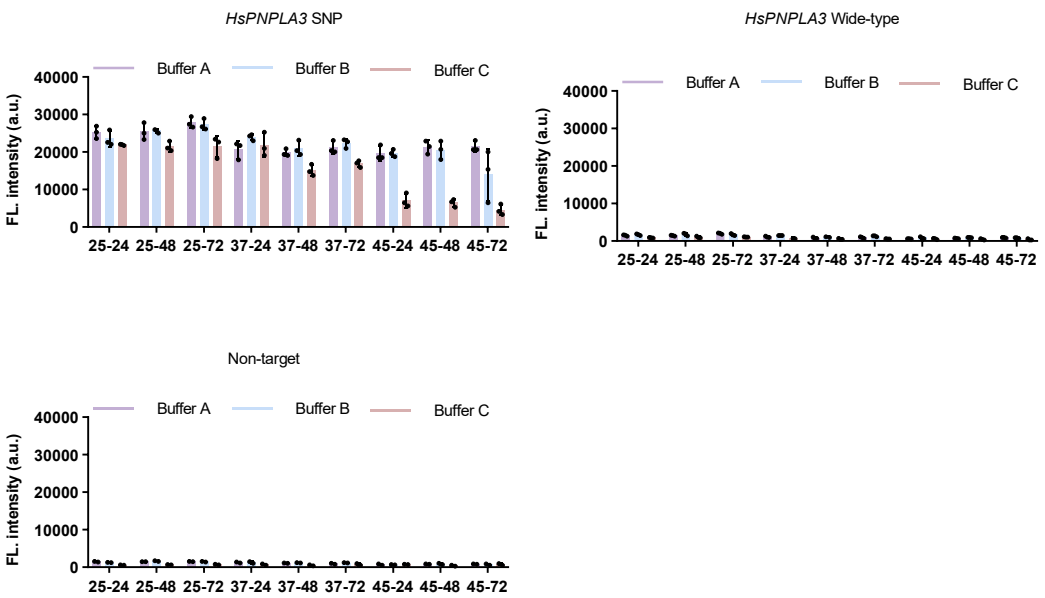

Fig. S13. Lyophilization process and detection of SNPs in *HsPNPLA3* using lyophilized mixtures. The lyophilized mixture comprises the crRNA, LbCas12a protein, and reaction buffer. a, Schematic workflow of manufacturing process of lyophilized mixture. b, Stability evaluation of lyophilized *HsPNPLA3* samples prepared in three different buffers under varying temperature and storage durations. Buffer A: 12.5% Sucrose, 8.33% Mannitol, 0.83% Tween 20, 1.66% Bovine Serum Albumin (BSA) , 50 mM Tris-HCl (pH 7.4), 2.5% Glycine; Buffer B: 12.5% Sucrose, 8,33% Mannitol, 0.83% Tween 20, 1.66% Bovine Serum Albumin (BSA), 50 mM Tris-HCl (pH 7.4); Buffer C: Nuclease-free water; X-axis: Temperature (°C) - Time (hours). Fluorescence intensities (mean ± *s.d.*) were calculated from three independent experiments (*n* = 3) and quantified in arbitrary units (a.u.).

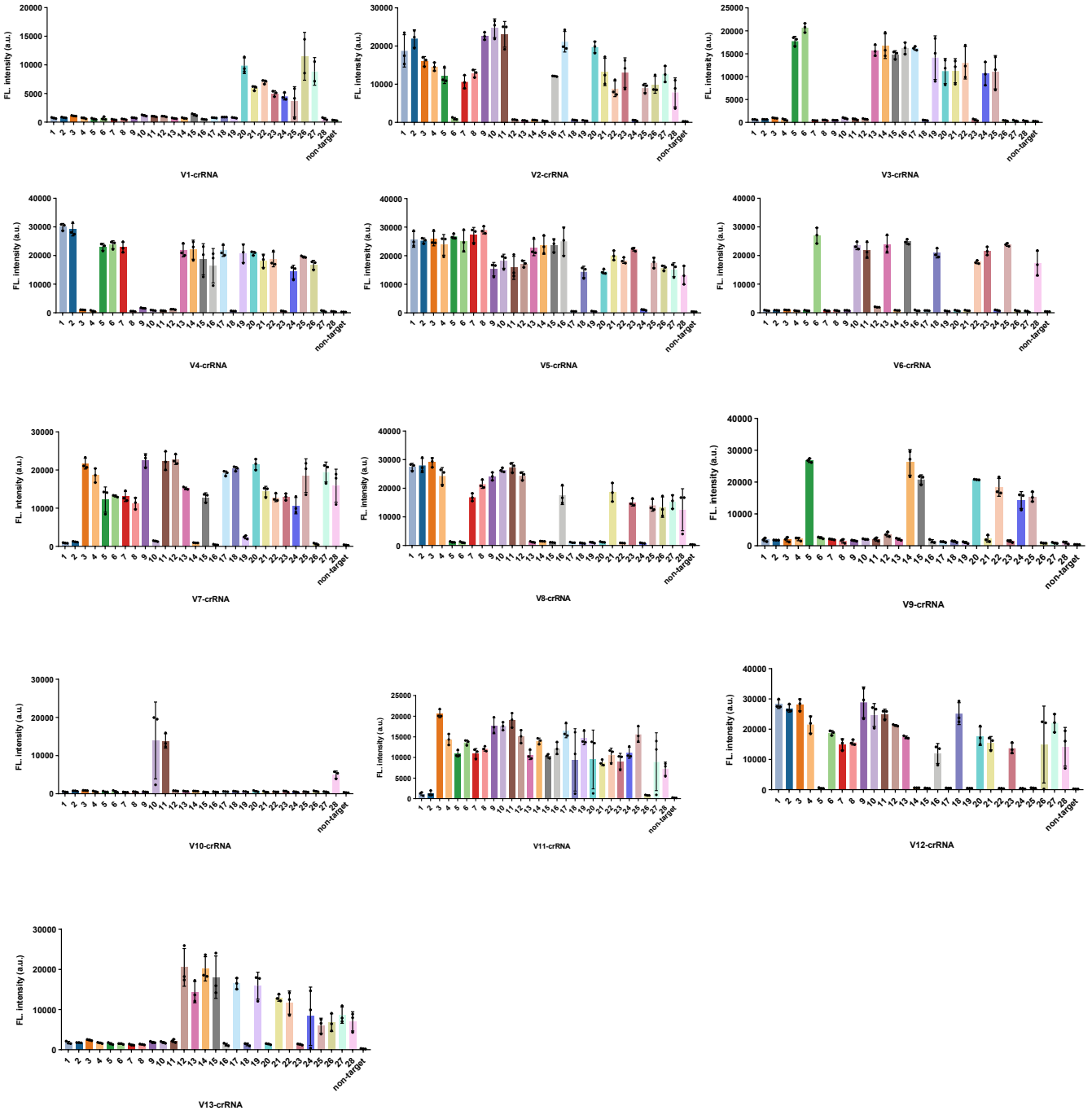

Fig. S14. Genetic classification of rice germplasm based on the SNIPER analysis. The X-axis shows different rice varieties. Each panel uses a distinct crRNA. Fluorescence intensities (mean ± *s.d.*) were calculated from three independent experiments (*n* = 3) and quantified in arbitrary units (a.u.).

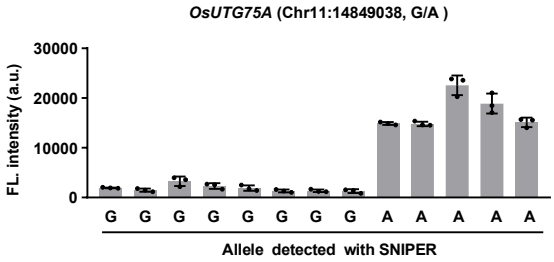

Fig. S15. Genotyping of functional SNPs associated with rice coleoptile elongation by SNIPER. The X-axis represents the nucleotide at the target SNP locus of the corresponding gene in different rice varieties. Fluorescence intensities (mean ± *s.d.*) were calculated from three independent experiments (*n* = 3) and quantified in arbitrary units (a.u.).

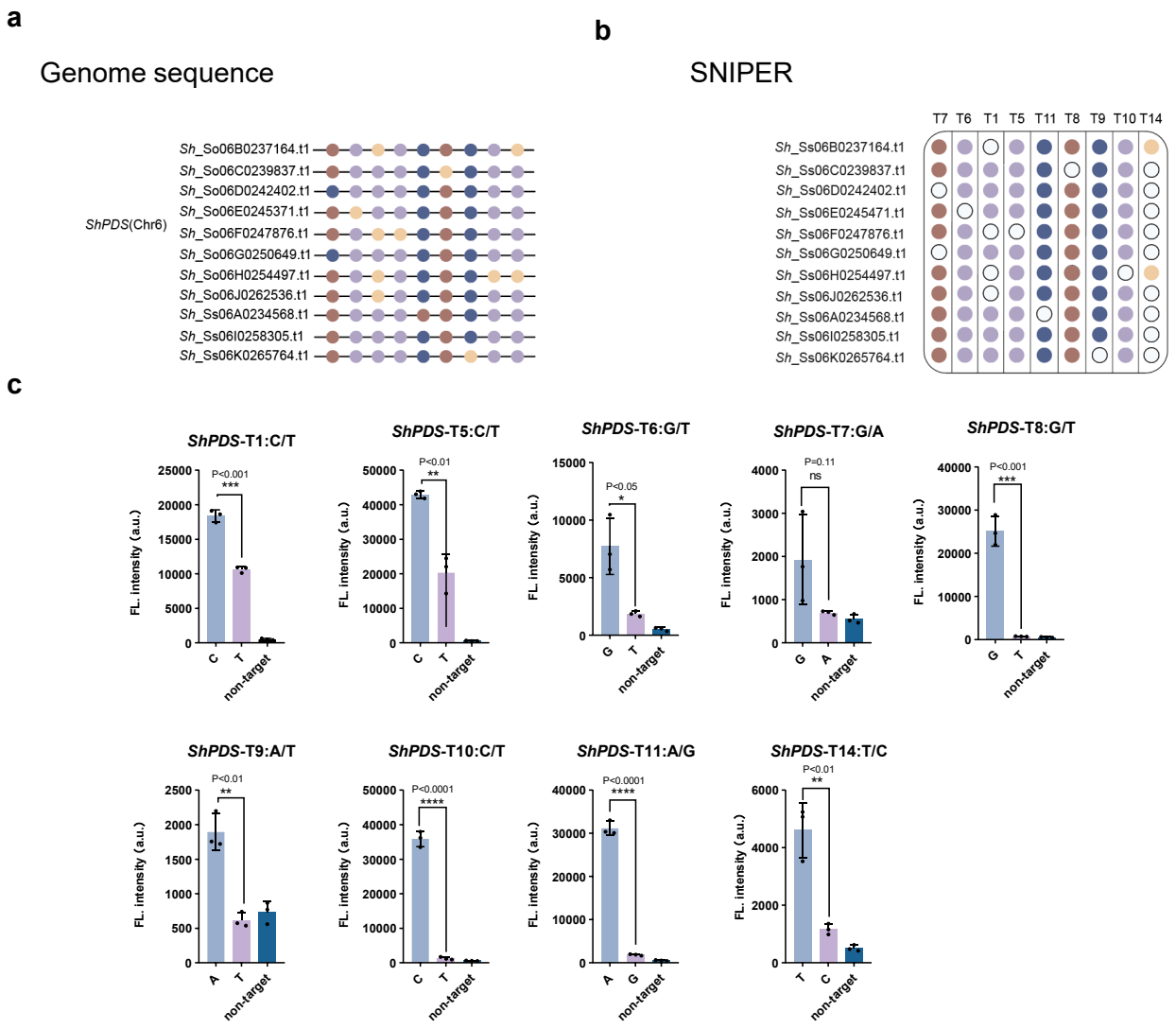

Fig. S16. Discrimination of distinct *ShPDS* alleles in sugarcane using the SNIPER assay. Discrimination of distinct *ShPDS* alleles. a, Genomic sequence of sugarcane; b, Results of the SNIPER assay; c, Specific fluorescence signals shown in Figure S16b. Fluorescence intensities (mean ± *s.d.*) were calculated from three independent experiments ($n = 3$) and quantified in arbitrary units (a.u.). *P* values were obtained using the two-tailed Student's t-test. $^{*}P < 0.05$, $^{**}P < 0.01$, $^{***}P < 0.001$, $^{****}P < 0.0001$, n.s., $P > 0.05$.

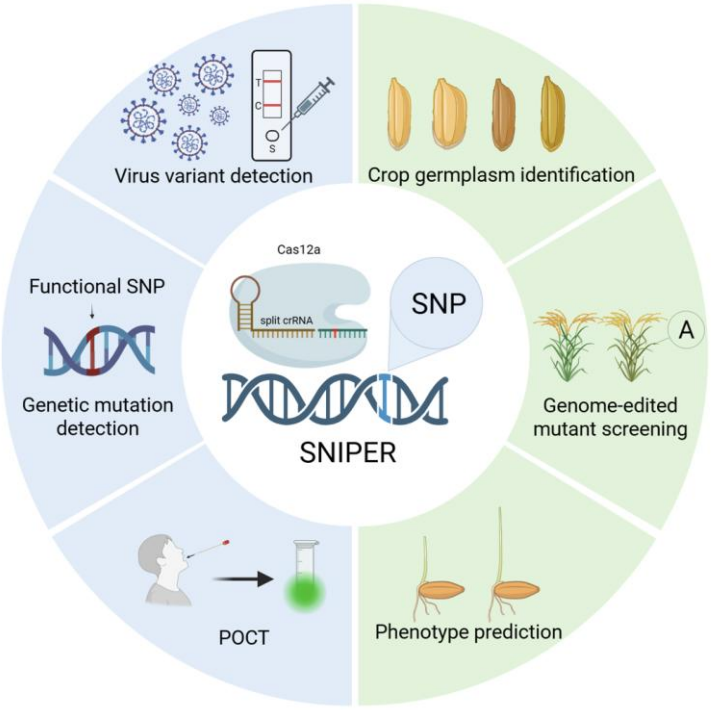

Fig. S17. Schematic diagram of diverse application scenarios for the SNIPER assay.